PCCP

Physical Chemistry Chemical Physics

This paper is published as part of a PCCP Themed Issue on:

New Frontiers in Surface-Enhanced Raman Scattering

Guest Editor: Pablo Etchegoin

Editorial

***Quo vadis* surface-enhanced Raman scattering?**
Phys. Chem. Chem. Phys., 2009
DOI: 10.1039/b913171j

Perspective

Surface-enhanced Raman spectroscopy of dyes: from single molecules to the artists' canvas
Kristin L. Wustholz, Christa L. Brosseau, Francesca Casadio and Richard P. Van Duyne, *Phys. Chem. Chem. Phys.*, 2009
DOI: 10.1039/b904733f

Communication

Tip-enhanced Raman scattering (TERS) of oxidised glutathione on an ultraflat gold nanoplate
Tanja Deckert-Gaudig, Elena Bailo and Volker Deckert, *Phys. Chem. Chem. Phys.*, 2009
DOI: 10.1039/b904735b

Papers

Self-assembly of α,ω-aliphatic diamines on Ag nanoparticles as an effective localized surface plasmon nanosensor based in interparticle hot spots
Luca Guerrini, Irene Izquierdo-Lorenzo, José V. Garcia-Ramos, Concepción Domingo and Santiago Sanchez-Cortes, *Phys. Chem. Chem. Phys.*, 2009
DOI: 10.1039/b904631c

Single-molecule vibrational pumping in SERS
C. M. Galloway, E. C. Le Ru and P. G. Etchegoin, *Phys. Chem. Chem. Phys.*, 2009
DOI: 10.1039/b904638k

Silver nanoparticles self assembly as SERS substrates with near single molecule detection limit
Meikun Fan and Alexandre G. Brolo, *Phys. Chem. Chem. Phys.*, 2009
DOI: 10.1039/b904744a

Gated electron transfer of cytochrome c_6 at biomimetic interfaces: a time-resolved SERR study
Anja Kranich, Hendrik Naumann, Fernando P. Molina-Heredia, H. Justin Moore, T. Randall Lee, Sophie Lecomte, Miguel A. de la Rosa, Peter Hildebrandt and Daniel H. Murgida, *Phys. Chem. Chem. Phys.*, 2009
DOI: 10.1039/b904434e

Investigation of particle shape and size effects in SERS using *T*-matrix calculations
Rufus Boyack and Eric C. Le Ru, *Phys. Chem. Chem. Phys.*, 2009
DOI: 10.1039/b905645a

Plasmon-dispersion corrections and constraints for surface selection rules of single molecule SERS spectra
S. Buchanan, E. C. Le Ru and P. G. Etchegoin, *Phys. Chem. Chem. Phys.*, 2009
DOI: 10.1039/b905846j

Redox molecule based SERS sensors
Nicolás G. Tognalli, Pablo Scodeller, Victoria Flexer, Rafael Szamocki, Alejandra Ricci, Mario Tagliazucchi, Ernesto J. Calvo and Alejandro Fainstein, *Phys. Chem. Chem. Phys.*, 2009
DOI: 10.1039/b905600a

Controlling the non-resonant chemical mechanism of SERS using a molecular photoswitch
Seth Michael Morton, Ebo Ewusi-Annan and Lasse Jensen, *Phys. Chem. Chem. Phys.*, 2009
DOI: 10.1039/b904745j

Interfacial redox processes of cytochrome b_{562}
P. Zuo, T. Albrecht, P. D. Barker, D. H. Murgida and P. Hildebrandt, *Phys. Chem. Chem. Phys.*, 2009
DOI: 10.1039/b904926f

Surface-enhanced Raman scattering of 5-fluorouracil adsorbed on silver nanostructures
Mariana Sardo, Cristina Ruano, José Luis Castro, Isabel López-Tocón, Juan Soto, Paulo Ribeiro-Claro and Juan Carlos Otero, *Phys. Chem. Chem. Phys.*, 2009
DOI: 10.1039/b903823j

SERS imaging of HER2-overexpressed MCF7 cells using antibody-conjugated gold nanorods
Hyejin Park, Sangyeop Lee, Lingxin Chen, Eun Kyu Lee, Soon Young Shin, Young Han Lee, Sang Wook Son, Chil Hwan Oh, Joon Myong Song, Seong Ho Kang and Jaebum Choo, *Phys. Chem. Chem. Phys.*, 2009
DOI: 10.1039/b904592a

Nanospheres of silver nanoparticles: agglomeration, surface morphology control and application as SERS substrates
Xiao Shuang Shen, Guan Zhong Wang, Xun Hong and Wei Zhu, *Phys. Chem. Chem. Phys.*, 2009
DOI: 10.1039/b904712c

SERS enhancement by aggregated Au colloids: effect of particle size
Steven E. J. Bell and Maighread R. McCourt, *Phys. Chem. Chem. Phys.*, 2009
DOI: 10.1039/b906049a

Towards a metrological determination of the performance of SERS media
R. C. Maher, T. Zhang, L. F. Cohen, J. C. Gallop, F. M. Liu and M. Green, *Phys. Chem. Chem. Phys.*, 2009
DOI: 10.1039/b904621f

Ag-modified Au nanocavity SERS substrates
Emiliano Cortés, Nicolás G. Tognalli, Alejandro Fainstein, María E. Vela and Roberto C. Salvarezza, *Phys. Chem. Chem. Phys.*, 2009
DOI: 10.1039/b904685m

Surface-enhanced Raman scattering studies of rhodanines: evidence for substrate surface-induced dimerization
Saima Jabeen, Trevor J. Dines, Robert Withnall, Stephen A. Leharne and Babur Z. Chowdhry, *Phys. Chem. Chem. Phys.*, 2009
DOI: 10.1039/b905008f

Characteristics of surface-enhanced Raman scattering and surface-enhanced fluorescence using a single and a double layer gold nanostructure
Mohammad Kamal Hossain, Genin Gary Huang, Tadaaki Kaneko and Yukihiro Ozaki, *Phys. Chem. Chem. Phys.*, 2009
DOI: 10.1039/b903819c

High performance gold nanorods and silver nanocubes in surface-enhanced Raman spectroscopy of pesticides
Jean Claudio Santos Costa, Rômulo Augusto Ando, Antonio Carlos Sant'Ana, Liane Marcia Rossi, Paulo Sérgio Santos, Márcia Laudelina Arruda Temperini and Paola Corio, *Phys. Chem. Chem. Phys.*, 2009
DOI: 10.1039/b904734d

Water soluble SERS labels comprising a SAM with dual spacers for controlled bioconjugation
C. Jehn, B. Küstner, P. Adam, A. Marx, P. Ströbel, C. Schmuck and S. Schlücker, *Phys. Chem. Chem. Phys.*, 2009
DOI: 10.1039/b905092b

Chromic materials for responsive surface-enhanced resonance Raman scattering systems: a nanometric pH sensor
Rômulo A. Ando, Nicholas P. W. Pieczonka, Paulo S. Santos and Ricardo F. Aroca, *Phys. Chem. Chem. Phys.*, 2009
DOI: 10.1039/b904747f

Interfacial redox processes of cytochrome b_{562}

P. Zuo,†[a] T. Albrecht,[b] P. D. Barker,[c] D. H. Murgida*[d] and P. Hildebrandt*[a]

Received 10th March 2009, Accepted 5th May 2009
First published as an Advance Article on the web 1st June 2009
DOI: 10.1039/b904926f

The anionic soluble heme protein cytochrome b_{562} was electrostatically immobilised on Ag electrodes coated with positively charged self-assembled monolayers of amino-terminated alkanethiols. The structure of the heme pocket, the redox equilibria, and the electron transfer dynamics were studied by stationary and time-resolved surface enhanced resonance Raman spectroscopy, complemented by cyclic voltammetry measurements of the interfacial redox process. The conformational and redox equilibria of the immobilised protein are compared to those of the cationic heme protein cytochrome c immobilised on negatively charged electrode coatings. Similarities and differences can be rationalised in terms of the respective electric fields at the interfaces of amino- and carboxyl-terminated electrode coatings. The heterogeneous electron transfer rate of cytochrome b_{562} only slightly increases with decreasing thickness from *ca.* 20 to 11 Å, implying that the electron tunneling is not the rate-limiting step. In contrast to cytochrome c on carboxyl-terminated monolayers, this behaviour cannot be attributed to protein re-orientation gating the heterogeneous electron transfer. Instead, it may reflect the interplay between interprotein electron transfer and heterogeneous electron transfer *via* protein orientations exhibiting particularly high tunneling probabilities for the electron exchange with the electrode.

Introduction

Long-distance electron transfer (ET) reactions play an essential role in many biological processes such as photosynthesis and respiration.[1] In these processes, electrons are transferred between proteins embedded in or (transiently) attached to biological membranes. Thus, the reactions take place under conditions that differ significantly from homogeneous ET reactions in solutions. Instead, biological ET reactions share various features of heterogeneous ET processes at electrodes. This is particularly true when redox proteins are immobilised on electrodes coated with self-assembled monolayers (SAMs) of functionalized mercaptoalkanes.[2,3] These SAMs can be considered as simple models for biological membranes with the alkyl chain and the tail groups representing the hydrophobic and polar or charged part of the lipid molecules, respectively. The tail groups can be chosen to immobilize the redox proteins mimicking the restricted mobility of proteins at biomembranes.[3] Furthermore, the electric field strengths at the SAM/solution interface are comparably high as those at the membrane/solution interface.[4,5] As a consequence, the ET processes of redox proteins immobilized on coated electrodes and biomembranes are subject to similar reaction conditions, specifically as far as the electrostatic forces acting on the proteins are concerned.

Due to these analogies, heterogeneous ET reactions of proteins have been in the focus of a large number of experimental studies, promoted by the development of sensitive electrochemical and spectroelectrochemical techniques.[1] Among them, surface enhanced resonance Raman (SERR) is a particularly powerful technique for studying heme proteins on coated Ag electrodes.[3,5,6] It combines the surface enhanced Raman (SER) and the molecular resonance Raman (RR) effects such that it selectively probes the vibrational spectrum of the heme cofactor solely of the immobilized proteins. In this way, one may obtain information about the heme structure and its potential-dependent changes and, in conjunction with the potential jump technique, the dynamics of the interfacial processes.

On the basis of SERR spectroscopic and electrochemical investigations, the most comprehensive set of data are available for the heme protein cytochrome c (Cyt-c).[3,5,6–25] Cyt-c is a soluble cationic protein that can be immobilized on coated electrodes *via* electrostatic interactions using SAMs of ω-carboxyl alkanethiols (COOH-SAM). It could be shown that at such devices the interfacial redox process results from a complex interplay been electron tunneling, rotational diffusion of the immobilized protein corresponding to transitions between orientations of different electron tunneling probability, and conformational changes affecting the redox potential.[22,25] The individual reaction steps, which can be selectively probed by (time-resolved) SERR spectroscopy using different excitation lines,[22] depend on the interfacial electric field. With increasing field strength, protein

[a] *Technische Universität Berlin, Institut für Chemie, Sekr. PC14, Straße des 17. Juni 135, D-10623 Berlin, Germany. E-mail: hildebrandt@chem.tu-berlin.de*
[b] *Imperial College London, Department of Chemistry, South Kensington Campus, London, United Kingdom SW7 2AZ*
[c] *University of Cambridge, Department of Chemistry, Lensfield Road, Cambridge, United Kingdom CB2 1EW*
[d] *Departamento de Química Inorgánica, Analítica y Química Física/ INQUIMAE-CONICET, Facultad de Ciencias Exactas y Naturales, Universidad de Buenos Aires. Ciudad Universitaria, Pab. 2, piso 1, C1428EHA-Buenos Aires, Argentina. E-mail: dhmurgida@qi.fcen.uba.ar*
† Present address: Chemical Dynamics Lab, RIKEN, 2-1 Hirosawa, Wako, Saitama 351-0198, Japan

re-orientation is slowed down and eventually becomes rate-limiting. A further increase of the field strength induces conformational changes in the heme pocket including the removal of the axial methionine ligand of the heme that causes the transition from the six-coordinated low spin (6cLS) to the five-coordinated high spin (5cHS) configuration.[3,9] The electric field dependence of the interfacial processes of Cyt-c can be well described on the basis of electrostatic models.[9,26] Accordingly, the thickness and the surface charge density are identified to be the crucial determinants of the electric field strength. The electric-field control of the interfacial redox process is not an unique property of Cyt-c. Similar effects on the structure and reaction dynamics that can be attributed to the interfacial electric field have also been observed for other redox proteins carrying a net positive surface charge as a prerequisite for immobilization to COOH-SAMs.[27–31]

In this work, we have extended the SERR spectroscopic analysis of interfacial redox processes to a protein possessing an excess negative surface charge, thus requiring immobilization to the electrode *via* amino-terminated mercaptoalkanes. We have chosen cytochrome b_{562} (Cyt-b_{562}), a small soluble b-type heme protein found in the periplasm of *Escherichia coli*.[32,33] Like Cyt-c, the heme group of Cyt-b_{562} is coordinated by a His and Met and also the redox potentials in solution are similar for both proteins.[34,35] Thus, the main difference in Cyt-b_{562} is the excess of negatively charged Asp and Glu residues as compared to Cyt-c with its positively charged Lys-rich binding domain.[35,36] This study is directed to analyse the effect of electrostatic interactions on the structural and electron transfer properties of the immobilized Cyt-b_{562} and to identify similarities and differences as compared to Cyt-c bound to COOH-SAMs.

Materials and methods

Materials

Cysteamine (NH_2-C2) purchased from Sigma-Aldrich as well as 6-amino-1-hexanethiol hydrochloride (NH_2-C6), 8-amino-1-octanethiol hydrochloride (NH_2-C8), and 11-amino-1-undecanethiol hydrochloride (NH_2-C11), all purchased from Dojindo, were used without further purification. KCl, K_2HPO_4, KH_2PO_4, and K_2SO_4 of high-purity grade were purchased from Sigma-Aldrich. Expression and purification of Cyt-b_{562} was reported previously.[37,38] The water used in all experiments was purified by a Millipore system and its resistance was 18.2 MΩ.

Methods

SERR spectra were measured with cw excitation of a Krypton ion laser (413 nm, Coherent Innova 300 K) and Argon ion laser (514 nm, Coherent Innova 300) using a confocal Raman microscope (LabRam, HR800) equipped with a liquid-nitrogen cooled CCD camera. The spectral resolution was 2 cm^{-1} and the increment per pixel was 0.57 cm^{-1}. The laser power at the sample was 2–6 mW. The average accumulation time for the stationary and time-resolved SERR spectra was 5 and 1.5 s, respectively. For the SERR experiments, a home-built electrochemical cell was used.[9,14]

Ag ring electrodes were treated by repetitive electrochemical oxidation/reduction electrochemical cycles in 0.1 M KCl to create a SER-active nanostructured surface. For coating with amino-terminated SAMs (NH_2-SAM), the roughened electrodes were immersed into a solution of amino-terminated mercaptoalkanes (1–2 mmol L^{-1}) in 4 : 1 (v/v) C_2H_5OH–H_2O at ambient temperature with average incubation times of 6, 50, and 30 h for NH_2-C2, NH_2-C6 (NH_2-C8), and NH_2-C11, respectively. Prior to measurement, the modified electrodes were rinsed thoroughly with ethanol and immersed into ethanol for 2–3 h to remove physically adsorbed amphiphiles and then dried under nitrogen.

The SERR experiments were carried out in aqueous solution containing a 12.5 mM potassium phosphate buffer (pH = 7.0) and 12.5 mM K_2SO_4. The concentration of Cyt-b_{562} was typically 0.1–0.2 μM. The electrode was kept at −100 mV *vs.* Ag/AgCl for about 1 h to establish adsorption equilibrium. All potentials cited in this work refer to the Ag/AgCl (3 M KCl) electrode. Time-resolved SERR experiments were carried out as described in detail previously.[14] The time response of the electrochemical cell was found to be shorter than 150 μs.

Subsequent to background subtraction stationary and time-resolved SERR spectra were subjected to a component analysis according to the procedure described elsewhere.[9] Cyclic voltammetry was carried out as described previously.[39] ET rate constants were determined according to Laviron′s method.[40]

Results

Conformational equilibria

The histidine/methionine ligation pattern of Cyt-b_{562} leads to a 6cLS configuration of the heme in both the reduced and oxidized form which is reflected by the characteristic marker bands in the RR spectrum of the protein in solution.[41] The SERR spectroscopic analysis is focused onto this spectral region since it allows quantification of the reduced and oxidized forms as well as adsorption-induced conformational changes that affect the heme pocket. Representative examples of SERR spectra of Cyt-b_{562} adsorbed on NH_2-C6-coated Ag electrode are shown in Fig. 1. The spectra mainly reflect the contributions from the native oxidized and reduced state which exhibit the same frequencies and relative intensities as observed in the RR spectra of the proteins in solution, indicating the preservation of the native heme pocket structure in the immobilized state. The same observations have been made for Cyt-c[9] even though, due to the opposite protein surface charge, electrostatic adsorption of Cyt-b_{562} and Cyt-c requires positively charged (NH_2-SAMs) and negatively charged SAMs (COOH-SAM), respectively. In analogy to Cyt-c, these native forms of Cyt-b_{562} are denoted as ferric and ferrous B1.

The most important marker bands that allow for distinguishing between both oxidation states originate from the ν_4 and ν_3 modes that, in the oxidized B1, are observed at 1370 and 1501 cm^{-1}, respectively, and undergo a *ca.* 10-cm^{-1} downshift upon reduction. Further redox-sensitive modes are

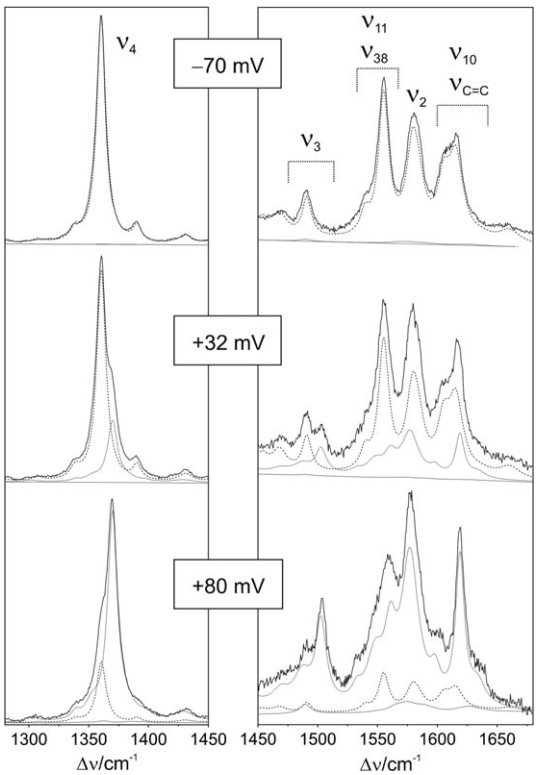

Fig. 1 SERR spectra of Cyt-b_{562} adsorbed on a Ag electrode coated with NH_2-C6 and measured with 413-nm excitation at different potentials. The component spectra of the reduced B1, oxidized B1, and oxidized B2(5cHS) states are represented by the black dashed, black dotted, and grey solid lines, respectively. The intensity scale of the right panel is expanded by a factor of 5.

the ν_{11}, ν_2, and ν_{10} which vary in frequency by up to 10 cm^{-1} and display considerable changes in the relative intensities upon redox transition. All these bands constitute the component spectra of the two B1 forms representing the basis for an initial global analysis of the experimental SERR spectra, which, however, does not afford satisfactory results. In fact, a careful inspection of the spectra reveals residual intensities at positions characteristic of a ferric 5cHS state, as for example at 1489 cm^{-1} corresponding to the mode ν_3. Such a species, denoted as B2(5cHS), was also observed for Cyt-c bound to negatively charged surfaces.[9] In fact, the component analysis including the spectral parameters adopted from the B2(5cHS) state of Cyt-c provides a consistent fit for all experimental SERR spectra.

The analysis of the SERR spectra of Cyt-b_{562} further indicates that the spectral contribution of the B2(5cHS) state increases with decreasing potential from less than 2% at +50 mV to *ca.* 4% at −80 mV for NH_2-C6. Only at very negative potentials (−400 mV), the B2(5cHS) species disappears but it is recovered after setting the electrode potential to a more positive value. Correspondingly, this species cannot be related to an irreversibly denatured protein state. For NH_2-C8 and NH_2-C11, the same potential-dependence is observed but the overall contribution increases with increasing chain length with a maximum value of *ca.* 12% at −80 mV for NH_2-C11.

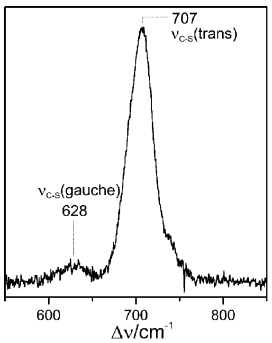

Fig. 2 SER spectrum of the NH_2-C6 SAM on an Ag electrode surface in the absence of immobilized protein, measured with 514-nm excitation. The spectrum displays the region of the C–S stretching modes.

The formation of the B2(5cHS) state does not result from the direct binding of the protein to the metal surface due to possible imperfections of the SAMs. First, in the potential range considered here, Ag surfaces in contact with aqueous solutions are covered by chemisorbed anions such that negatively charged proteins like Cyt-b_{562} are repelled rather than attracted. Second, SAM imperfections are known to decrease with increasing chain length of the amphiphiles whereas the relative contribution of B2(5cHS) varies in the opposite order. Third, the NH_2-SAMs form a largely ordered structure with the *trans* conformation being the prevailing form. This is demonstrated by the SER spectrum of NH_2-C6 SAM, measured in the absence of protein with 514-nm excitation. This spectrum displays the bands attributable to the C–S stretching modes of the *trans* and *gauche* conformation with an intensity ratio of *ca.* 15 : 1 (Fig. 2). No time-dependent changes in the spectrum were observed during continuous laser irradiation with 514 nm (6 mW) or 413 nm (4 mW) for 5 min, *i.e.*, conditions sufficient to measure SERR spectra of Cyt-b_{562} with an acceptable signal-to-noise ratio.

Redox equilibria

The systematic measurements of SERR spectra as a function of the electrode potential allow us to determine the redox equilibria and thus the redox potentials of the immobilized

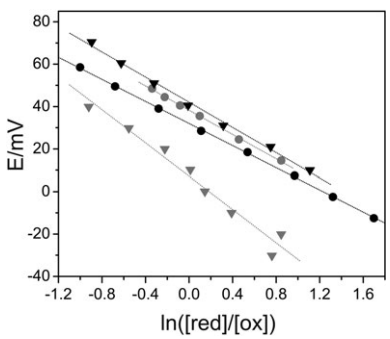

Fig. 3 Nernstian plots for the redox processes of Cyt-b_{562} adsorbed on Ag electrodes coated with different NH_2-SAMs: NH_2-C11, black triangles; NH_2-C8, grey circles; NH_2-C6, black circles; NH_2-C2, grey triangles. The data were obtained from the component analyses of the potential-dependent SERR spectra.

Table 1 Thermodynamic and kinetic parameters of the redox process of Cyt-b_{562} on NH2-SAM-coated Ag electrodes

	E^0/mV[a]		k_{app}/s^{-1}	
SAM	SERR	CV	SERR[bc]	CV[cd]
NH_2-C2	+7 (0.7)	N.d.[e]	N.d.[e]	N.d.[e]
NH_2-C6	+32 (0.98)	32	132 (~130)	124 (108)
NH_2-C8	+38 (0.92)	n.d.[e]	108	N.d.[e]
NH_2-C11	+42 (0.88)	39	68	76 (68)

[a] Values for the formal number of transferred electrons are given in parentheses. The error for E^0 is estimated to be lower than $|\pm 5|$ mV. [b] Relaxation rate constants determined from a mono-exponential fit to the experimental data. [c] The error is estimated to be ± 10 s^{-1}. The values in parentheses refer to k_{app} determined in the presence of 6.5% sucrose in the bulk solution. [d] The values are obtained after multiplying the k_{ET}, derived from the CV measurements, by a factor of 2. The values in parentheses refer to k_{app} determined in the presence of 6.5% sucrose in the bulk solution. [e] N.d., not determined.

proteins. The Nernstian plots obtained from the quantitative analysis of the SERR spectra (Fig. 3) display nearly ideal linear correlations with slopes corresponding to a number of transferred electrons between 0.7 and 1.0 for the various chain-lengths (Table 1). The redox potentials are more positive than that of the protein in solution and this potential shift distinctly increases with increasing chain length. (Table 1 and Fig. 4). The same tendency is also observed in CV experiments.

Electron transfer dynamics

To probe the kinetics of the immobilized Cyt-b_{562}, time-resolved experiments were carried out with potential jumps in a range from *ca.* −70 to +50 mV. In this range, the equilibrium concentration of the B2(5cHS) state varies. The conformational transition between the B1 and B2 states, however, takes place within minutes and thus on a much longer time scale than the interfacial ET (<100 ms). Accordingly, we can restrict the analysis of the ET process to the reactions of the native B1 state.

The potential jumps were chosen such that the final potential E_f corresponds to the redox potential at the respective NH_2-SAM, *i.e.*, the driving force for the ET was equal to 0 eV, whereas the initial potential E_i was chosen to be more negative. Thus, the resultant relaxation process that was probed by time-resolved SERR spectroscopy referred to the

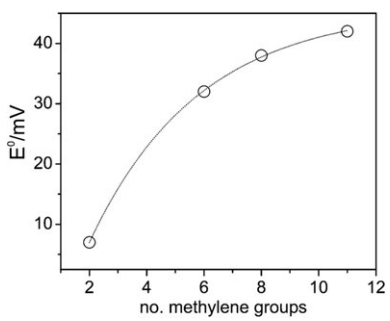

Fig. 4 Redox potentials (E^0) of Cyt-b_{562} on Ag electrodes coated with NH_2-SAMs of different chain lengths (number of methylene groups in the chain). The data were obtained from the component analyses of the potential-dependent SERR spectra.

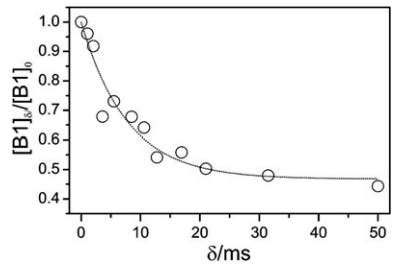

Fig. 5 Time-dependent changes of the relative concentrations of the reduced Cyt-b_{562} (B1) adsorbed on an Ag electrode coated with NH_2-C6. The data were obtained from time-resolved SERR spectra measured with 413-nm excitation at different delay times after the potential jump from −18 mV to the apparent redox potential (+32 mV).

oxidation of the native ferrous B1 state. For small potential jumps, *i.e.* $\Delta E = E_f - E_i \cong -50$ mV, the temporal evolution of the ferrous B1 state could be satisfactorily described by a single exponential decay such that the reciprocal slope of the semilogarithmical plot of the concentration changes over the delay time corresponds to the relaxation rate constant k_{app} (Fig. 5). In case of a pure ET reaction, *i.e.* a one-step relaxation process, k_{app} is equal to the sum of the rate constants for the forward and backward reactions which at $\Delta G = 0$ eV are equal and thus $k_{app} = 2 \cdot k_{ET}$.

These relaxation rate constants increase with decreasing chain length corresponding to 68, 108, and 132 s^{-1} for NH_2-C11, NH_2-C8 and NH_2-C6 SAMs, respectively. Very similar results were obtained by CV measurements leading to k_{app} values of 76 and 124 s^{-1} for NH_2-C11 and NH_2-C6, respectively (Fig. 6, Table 1). In all CVs the peak current varies linearly with the scan rate indicating a surface-confined process.

No reliable kinetic data could be extracted from CV measurements from electrodes coated with NH_2-C2 SAMs. For such a short chain length, hydrophobic interactions

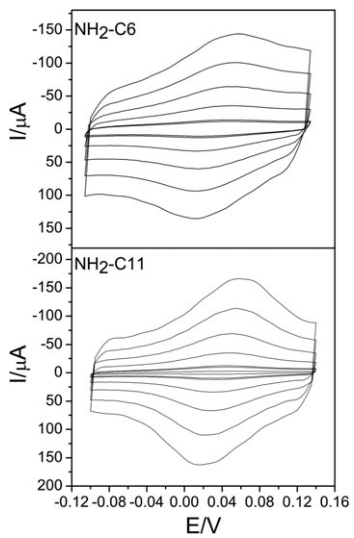

Fig. 6 Cyclic voltammograms of Cyt-b_{562} on Ag electrodes coated with NH_2-C6 and NH_2-C11, recorded with different scan rates (20, 80, 100, 300, 600, 1000, and 1500 mV s^{-1}).

between the alkyl chains are too weak to ensure a well-ordered SAM structure and the amino group may compete with the thiol function for binding to the Ag surface. The poorly ordered structure of NH_2-C2 is reflected by the strong intensity increase of the *gauche vs.* the *trans* marker band in the SER spectrum.[42]

The increase of k_{app} by a factor of *ca.* 2 from NH_2-C11 to NH_2-C6 SAMs cannot be rationalized in terms of the distance-dependence of electron tunneling which predicts an increase by *ca.* four orders of magnitude. In this respect, the kinetic data of Cyt-b_{562} resemble those obtained for Cyt-c immobilized on COOH-SAMs for which protein (re-)orientation has been shown to control the ET process in the non-tunneling regime.[22] This re-orientation was found to be slowed down upon increasing the viscosity of the bulk solution, corresponding to a decrease of the relaxation rate constant by a factor of 2 in the presence of 6.5% sucrose. To check whether a similar mechanism also holds for Cyt-b_{562} on NH_2-SAMs, we have probed the intensity ratios of A_{1g} and B_{1g} modes using 514-nm excitation. However, these experiments did not reveal any potential- and time-dependent changes of the relative band intensities that would reflect changes of the orientational distribution of Cyt-b_{562}. Furthermore, a sucrose concentration of 6.5% causes only a 10% decrease of the rate constants determined by time-resolved SERR spectroscopy and CV measurements. A more substantial decrease to about 60% and 30% was only observed when the sucrose concentration was raised significantly to 20% and 34%, respectively. At such high sucrose concentrations, however, a structural perturbation of the SAM/protein complex cannot be ruled although the band positions and intensities in the SERR spectra were not affected.

Upon applying larger potential jumps with $\Delta E \cong -100$ mV, the ET dynamics of Cyt-b_{562} become complex and a single exponential function does not provide an adequate description for the relaxation process. Moreover, in some experiments a "lag" phase was observed at very early delay times such that the ET process starts after a delay between 2 to 6 ms. We do not have a satisfactory explanation for this effect, but we can rule out interference with the time constant of the electrochemical cell which was determined to be <150 μs. A lag phase was never noted for small potential jumps such that we have restricted the analysis of the interfacial ET dynamics of Cyt-b_{562} to experiments with $\Delta E = E_f - E_i \cong -50$ mV.

Discussion

Redox and conformational equilibria

The interfacial processes of Cyt-b_{562} display some similarities but also a few striking differences compared to Cyt-c. The redox potentials determined for the immobilized proteins reveal the expected shifts E_{RC} with respect to the redox potentials in solution.[9] The absolute values of E_{RC} increase with increasing SAM lengths and are quite similar for both proteins. However, the signs are different, *i.e.*, positive for Cyt-b_{562} on NH_2-SAMs and negative for Cyt-c on COOH-SAMs.

For both proteins, the immobilization on electrodes coated with SAMs, albeit oppositely charged, provide a biocompatible environment since the native heme pocket structure is preserved. However, both proteins undergo a reversible conformational transition under dissociation of the axial methionine ligand leading to the B2(5cHS) state. For Cyt-c, this equilibrium is shifted towards the B2(5cHS) state by increasing the interfacial electric field strength.[9] Thus, it is tempting to assume that the B2(5cHS) formation of Cyt-b_{562} is induced by the interfacial electric field as well. For COOH-SAMs the B2(5cHS) content increases with decreasing chain length and increasing electrode potential.[3,9] Here we note a striking difference for Cyt-b_{562} immobilised on the positively charged SAM surface with the relative contribution of B2(5cHS) increasing with decreasing potential and increasing chain length.

Electric field strengths at the SAM/protein interface

Evidently, the electric field strength in the SAM/protein interface varies in opposite directions for COOH- and NH_2-SAMs. To rationalize this difference we refer to the electrostatic model employed for Cyt-c immobilized on COOH-SAMs.[9] In that case it was shown that the electric field strength on the SAM surface E_F is given by

$$E_F = \frac{\varepsilon_0 \varepsilon_S \kappa E_{RC} - \sigma_C - \sigma_{RC}}{\varepsilon_0 \varepsilon_C} \qquad (1)$$

where ε_S and ε_C are the dielectric constants in solution and in the SAM, respectively; κ denotes the reciprocal Debye length and ε_0 the permittivity. The quantities σ_C and σ_{RC} are the charge densities on SAM surface and at the redox center, respectively. For a qualitative comparison of the electric field strengths at COOH-SAM and NH_2-SAM interfaces, it is sufficient to consider only the first and the second term as the absolute value of the third one is distinctly smaller.[9] By inserting the respective values for ε_S, ε_C, κ, and ε_0, we re-write eqn (1) according to

$$E_F = \frac{\varepsilon_S \kappa}{\varepsilon_C} E_{RC} - \frac{1}{\varepsilon_0 \varepsilon_C} \sigma_C \approx (0.6 \cdot E_{RC} - \sigma_C) \cdot 10^{10} \text{ V m}^{-1} \qquad (2)$$

with E_{RC} and σ_C expressed in V and C m^{-2}, respectively. E_{RC} and σ_C have the same sign, *i.e.*, they are positive for NH_2-SAMs but negative for COOH-SAMs. The charge density σ_C is directly related to the pK_A value of the tail group, corresponding to

$$\sigma_C(NH_2) = \frac{1}{1 + 10^{pH - pK_A}} \sigma_{C,max}(NH_2) \qquad (3)$$

for NH_2-SAMs and

$$\sigma_C(COOH) = \frac{10^{pH - pK_A}}{1 + 10^{pH - pK_A}} \sigma_{C,max}(COOH) \qquad (4)$$

for COOH-SAMs with $\sigma_{C,max}(NH_2)$ and $\sigma_{C,max}(COOH)$ denoting the respective maximum surface charge densities. The pK_A values for COOH-SAMs are at around 8 and increase slightly with increasing chain length.[43–46] Thus, according to eqn (4), the absolute values of $\sigma_C(COOH)$ decrease with longer chains at pH 7. The concomitant increase

of $|E_{RC}|$ then causes a rapid decay of the electric field strength with increasing chain length (see eqn (2)). For NH_2-SAMs, the pK_A values are at *ca.* 6.5 and seem to increase as well with the chain length,[47–50] which at pH 7, however, corresponds to an increase of the field strength with increasing chain length. Furthermore, assuming $\sigma_{C,max}(NH_2) \cong \sigma_{C,max}(COOH)$, σ_C is the dominant term in eqn (2) for NH_2-SAMs such that the contribution of the first term remains small and the absolute value of the electric field strength is distinctly higher than for COOH-SAMs.

These considerations can account for the increase of the B2(5cHS) content of Cyt-b_{562} in the order NH_2-C6 < NH_2-C8 < NH_2-C11 as well as for the opposite tendency of the B2(5cHS) content in Cyt-c on COOH-SAMs. Also the potential-dependence of the conformational equilibria is different for Cyt-b_{562} on NH_2-SAMs and Cyt-c on COOH-SAMs, which can be qualitatively understood in view of the potential-dependence of the pK_A. With decreasing potential, the increased electron density on the metal destabilizes the carboxylate groups of COOH-SAMs, corresponding to an increase of the pK_A and a decrease of the electric field strength. Correspondingly, the protonated amino groups will be stabilized concomitant with an increase of the pK_A and an increase of the electric field. These tendencies are consistent with the experimental findings that the B2(5cHS) content increases with more negative potentials for Cyt-b_{562} on NH2-SAMs but increases in the opposite direction for Cyt-c on COOH-SAMs.[3,9]

The dynamics of the interfacial redox process

The dynamics of the ET process of Cyt-c on COOH-SAMs can be well understood in terms of orientation-dependent tunneling probabilities of the immobilized proteins.[22,25] Electrostatic adsorption of Cyt-c leads to a distribution among various orientations, each of them associated with different electron tunneling probabilities.[25] At long chain lengths such as COOH–C16, corresponding to weak electric fields, the activation barrier for orientational changes of the protein is low and thus re-orientation dynamics is fast ($>6000\ s^{-1}$) compared to electron tunneling ($0.07\ s^{-1}$).[22] With decreasing SAM length, the tunneling rate increases exponentially and the re-orientation rate decreases due to the increase of the electric field dependent activation energy. Thus, the distance-dependence of re-orientation and electron tunneling rate constants display a crossing point below a chain length of COOH–C11. In this region and for shorter SAMs, the overall ET is controlled by the electric-field dependent orientational distribution and the re-orientational dynamics.

For Cyt-b_{562}, the relaxation constant determined for NH_2-C11 ($72\ s^{-1}$) is comparable to that for Cyt-c at COOH–C11 ($83\ s^{-1}$). With decreasing chain length, the rate constant only slightly increases such that at NH_2-C6 the relaxation constant is even lower ($130\ s^{-1}$) than for Cyt-c at the corresponding COOH–C6 SAM ($250\ s^{-1}$). In this case, no potential- and time-dependent orientational changes could be detected. Although we cannot rule out that the orientational distribution is too narrow to allow for SERR-detection with 514-nm excitation, it appears to be more likely that the quasi distance-independence of the ET rate constant has a different origin. Waldeck and coworkers suggested a change of the ET mechanism from a distance-dependent non-adiabatic to a distance-independent adiabatic regime,[15,17,18] which has in fact been demonstrated for Cyt-c coordinatively bound to pyridine-terminated SAMs[19] but cannot account for electrostatically adsorbed Cyt-c.[22]

For Cyt-b_{562} an alternative explanation is appealing in view of the fact that, at pH 7, the electric field strength experienced by the adsorbed protein is distinctly higher than for Cyt-c on COOH-SAMs. Thus, one may assume that, unlike to Cyt-c on COOH-SAMs, the mobility of the bound Cyt-b_{562} on NH_2-SAMs is essentially blocked due to a significantly higher activation energy for rotational diffusion on the SAM surface. As a result, the orientational distribution is "frozen" and the heterogeneous ET of Cyt-b_{562} will proceed preferentially *via* those orientations that are associated with the highest electron tunneling probabilities. These orientations may also constitute efficient ET "channels" for the remainder of protein orientations associated with low tunneling probabilities, implying that for these protein populations interprotein ET precedes the heterogeneous ET. This mechanism should be reflected by a rather complex kinetic behavior. If, however, the relative concentration of efficient ET channels is low, the overall redox process may be reasonably well approximated by a single exponential function (see Fig. 5). Then, the experimentally determined ET rate is limited by interprotein ET between the adsorbed proteins rather then by the fast heterogeneous ET *via* the distinguished protein orientations. This model is consistent with the very weak viscosity effect and the failure to detect orientational changes of the adsorbed Cyt-b_{562} by SERR spectroscopy. A similar mechanism has been previously suggested for Cyt-c embedded in polyelectrolyte layers on electrodes that as well are devices of restricted protein mobility.[51,52]

Conclusions

1. NH_2-SAMs provide a biocompatible coating of electrodes for immobilizing anionic proteins without denaturation. Conformational changes of Cyt-b_{562} as reflected by the SERR spectra are reversible and refer to the dissociation of the Met-ligand from the heme iron. This conformational change depends on the electric field strength in the SAM/protein interface similar to previous findings for Cyt-c on COOH-SAM coated electrodes.

2. However, the conformational equilibria of Cyt-b_{562} display the opposite distance- and potential-dependence as Cyt-c which can be rationalized in terms of the respective electric field strength and sign on NH_2- and COOH-SAMs.

3. Correspondingly, the experimentally determined redox potentials display the opposite tendencies for Cyt-b_{562} and Cyt-c on electrodes coated with NH_2- and COOH-SAMs, respectively.

4. Unlike Cyt-c on COOH-SAMs, the Cyt-b_{562}/NH_2-SAM system does not provide evidence for protein reorientation being the rate-limiting step in the distance-independent ET transfer regime. Instead, heterogeneous ET may mainly occur *via* "frozen" protein orientations exhibiting high tunneling

probabilities for the electron exchange with electrode such that interprotein ET between the immobilized proteins is the rate-limiting event.

Acknowledgements

This work was supported by the Volkswagen-Stiftung (I 80816; P. H., D. H. M.), ANPCyT (PICT2006-459; PICT2007-00314; D. H. M.), and the DFG (Cluster of Excellence ''Unicat'', P. H.). Z. P. acknowledges a fellowship from the Alexander-von-Humboldt Stiftung.

References

1 P. N. Bartlett, *Bioelectrochemistry*, John Wiley & Sons, Chichester, 2008.
2 A. Ulman, *Chem. Rev*., 1996, **96**, 1533.
3 D. H. Murgida and P. Hildebrandt, *Phys. Chem. Chem. Phys*., 2005, **7**, 3773.
4 R. J. Clarke, *Adv. Colloid Interface Sci*., 2001, **89–90**, 263.
5 D. H. Murgida and P. Hildebrandt, *Acc. Chem. Res*., 2004, **37**, 854.
6 D. H. Murgida and P. Hildebrandt, *Chem. Soc. Rev*., 2008, **37**, 937.
7 A. El Kasmi, J. M. Wallace, E. F. Bowden, S. M. Binet and R. J. Linderman, *J. Am. Chem. Soc*., 1998, **120**, 225.
8 D. H. Murgida and P. Hildebrandt, *Angew. Chem., Int. Ed*., 2001, **40**, 728.
9 D. H. Murgida and P. Hildebrandt, *J. Phys. Chem. B*, 2001, **105**, 1578.
10 A. Avila, B. W. Gregory, K. Niki and T. M. Cotton, *J. Phys. Chem. B*, 2000, **104**, 2759.
11 M. J. Tarlov and E. F. Bowden, *J. Am. Chem. Soc*., 1991, **113**, 1847.
12 L. Rivas, D. H. Murgida and P. Hildebrandt, *J. Phys. Chem. B*, 2002, **106**, 4823.
13 D. H. Murgida and P. Hildebrandt, *J. Mol. Struct*., 2001, **565–566**, 97.
14 D. H. Murgida and P. Hildebrandt, *J. Am. Chem. Soc*., 2001, **123**, 4062.
15 J. J. Wei, H. Y. Liu, A. R. Dick, H. Yamamoto, Y. F. He and D. H. Waldeck, *J. Am. Chem. Soc*., 2002, **124**, 9591.
16 K. Ataka and J. Heberle, *J. Am. Chem. Soc*., 2004, **126**, 9445.
17 J. J. Wei, H. Y. Liu, D. E. Khoshtariya, H. Yamamoto, A. Dick and D. H. Waldeck, *Angew. Chem., Int. Ed*., 2002, **41**, 4700.
18 J. J. Wei, H. Y. Liu, K. Niki, E. Margoliash and D. H. Waldeck, *J. Phys. Chem. B*, 2004, **108**, 16912.
19 D. H. Murgida, P. Hildebrandt, J. Wei, Y. F. He, H. Y. Liu and D. H. Waldeck, *J. Phys. Chem. B*, 2004, **108**, 2261.
20 D. Millo, A. Bonifacio, A. Ranieri, M. Borsari, C. Gooijer and G. van der Zwan, *Langmuir*, 2007, **23**, 9898.
21 N. Wisitruangsakul, I. Zebger, K. H. Ly, D. H. Murgida and P. Hildebrandt, *Phys. Chem. Chem. Phys*., 2008, **10**, 5276.
22 A. Kranich, K. H. Ly, P. Hildebrandt and D. H. Murgida, *J. Am. Chem. Soc*., 2008, **130**, 9844.
23 K. L. Davis and D. H. Waldeck, *J. Phys. Chem. B*, 2008, **112**, 12498.
24 H. Yue, D. H. Waldeck, K. Schrock, D. Kirby, K. Knorr, S. Switzer, J. Rosmus and R. A. Clark, *J. Phys. Chem. C*, 2008, **112**, 2514.
25 D. A. Paggi, D. F. Martín, A. Kranich, P. Hildebrandt, M. Martí and D. H. Murgida, *Electrochim. Acta*, 2009, **54**, 4963.
26 C. P. Smith and H. S. White, *Anal. Chem*., 1992, **64**, 2398.
27 A. Kranich, D. Naumann, F. P. Molina-Heredia, H. J. Moore, T. R. Lee, S. Lecomte, M. A. de la Rosa, P. Hildebrandt and D. H. Murgida, *Phys. Chem. Chem. Phys*., 2009, DOI: 10.1039/b904434e, this issue.
28 L. Rivas, C. M. Soares, A. M. Baptista, J. Simaan, R. DiPaolo, D. H. Murgida and P. Hildebrandt, *Biophys. J*., 2005, **88**, 4188.
29 J. Simaan, D. H. Murgida and P. Hildebrandt, *Biopolymers*, 2002, **67**, 331.
30 L. Rivas, D. H. Murgida and P. Hildebrandt, *J. Mol. Struct*., 2001, **565–566**, 193.
31 S. Todorovic, C. Jung, P. Hildebrandt and D. H. Murgida, *JBIC, J. Biol. Inorg. Chem*., 2006, **11**, 119.
32 E. Itagaki and L. P. Hager, *J. Biol. Chem*., 1966, **241**, 3687.
33 H. Nikkila, R. B. Gennis and S. G. Sligar, *Eur. J. Biochem*., 1991, **202**, 309.
34 P. D. Barker, J. L. Butler, P. de Oliveira, H. A. O. Hill and N. I. Hunt, *Inorg. Chim. Acta*, 1996, **252**, 71.
35 *Cytochrome c. A Multidisciplinary Approach*, ed. R. A. Scott and A. G. Mauk, University Science, Mill Valley, 1995.
36 K. Hamada, P. H. Bethge and S. F. Mathews, *J. Mol. Biol*., 1995, **247**, 947.
37 P. D. Barker, E. P. Nerou, S. M. V. Freund and I. M. Fearnley, *Biochemistry*, 1995, **34**, 15191.
38 J. K. Rice, I. M. Fearnley and P. D. Barker, *Biochemistry*, 1999, **38**, 16847.
39 J. J. Feng, P. Hildebrandt and D. H. Murgida, *Langmuir*, 2008, **24**, 1583.
40 E. Laviron, *J. Electroanal. Chem*., 1979, **101**, 19.
41 R. B. Srivastava, C. Pace and N.-T. Yu, *J. Raman Spectrosc*., 1981, **11**, 20.
42 A. Michota, A. Kudelski and J. Bukowska, *J. Raman Spectrosc*., 2001, **32**, 345.
43 C. D. Bain and G. M. Whitesides, *Langmuir*, 1989, **5**, 1370.
44 J. Wang, L. M. Frostman and M. D. Ward, *J. Phys. Chem*., 1992, **96**, 5224.
45 K. Shimazu, T. Teranishi, K. Sugihara and K. Uosaki, *Chem. Lett*., 1998, 669.
46 H. S. White, J. D. Peterson and K. J. Stevenson, *J. Phys. Chem. B*, 1998, **102**, 2930.
47 D. V. Vezenov, A. Noy, L. F. Rozsnyai and C. M. Lieber, *J. Am. Chem. Soc*., 1997, **119**, 2006.
48 M. L. Wallwork and D. A. Smith, *Langmuir*, 2001, **17**, 1126.
49 H. Munakata, D. Oyamatsu and S. Kuwabata, *Langmuir*, 2004, **20**, 10123.
50 X. W. Cao, *J. Raman Spectrosc*., 2005, **36**, 250.
51 M. K. Beissenhirtz, F. W. Scheller, W. F. M. Stöcklein, D. Kurth, H. Möhwald and F. Lisdat, *Angew. Chem., Int. Ed*., 2004, **43**, 4357.
52 I. Weidinger, D. H. Murgida, W. Dong, H. Möhwald and P. Hildebrandt, *J. Phys. Chem. B*, 2006, **110**, 522.

